Near-zero 33 S and 36 S anomalies in Pitcairn basalts suggest Proterozoic sediments in the EM-1 mantle plume

Jabrane Labidi, James W. Dottin Ill, M Clog, C Hemond, P Cartigny

Near-zero ^{33}S and ^{36}S anomalies in Pitcairn basalts suggest Proterozoic sediments in the EM-1 mantle plume

Labidi, J.[1] Dottin, J. III[2], Clog, M.[3] Hemond, C.[4], Cartigny, P.[1]

1 *Université de Paris, Institut de Physique du Globe de Paris, CNRS, F-75005 Paris, France.*
2 Department of Geology, University of Maryland, College Park, MD 20742, United States
3 Scottish Universities Environmental Research Center, East Kilbride, United Kingdom
4 Université Brest, CNRS, IUEM, UMR 6538 Laboratoire Géosciences Océan, Rue Dumont d'Urville, 29280 Plouzané, France

Highlights : Sulfur isotopes, Pitcairn, Recycling, Global geodynamics

Abstract

Volcanic rocks erupted among Pitcairn seamounts sample a mantle plume that exhibits an extreme Enriched Mantle-1 signature. The origin of this peculiar mantle endmember remains contentious, and could involve the recycling of marine sediments of Archean or Proterozoic ages, delaminated units from the lower continental crust, or metasomatized peridotites from a lithospheric mantle. Here, we report the sulfur multi-isotopic signature (^{32}S, ^{33}S, ^{34}S, ^{36}S) of 15 fresh submarine basaltic glasses from three Pitcairn seamounts. We observe evidence for magmatic degassing of sulfur from melts erupted ~2,000 meters below seawater level (mbsl). Sulfur concentrations are correlated with eruption depth, and range between 1300 ppm S (collected ~ 2,500 mbsl) and 600 ppm S (~2,000 mbsl). The $\delta^{34}S$ values can be accounted for under equilibrium isotope fractionation during degassing, with $\alpha_{gas\text{-}melt}$ between 1.0020 and 1.0001 and starting $\delta^{34}S$ values between –0.9‰ and +0.6‰. The $\delta^{34}S$ estimates are similar or higher than MORB signatures, suggesting the contribution of recycled sulfur with

a ~ 1‰ ^{34}S enrichment compared to pacific upper mantle. The $\Delta^{33}S$ and $\Delta^{36}S$ signatures average at +0.024±0.007‰ and +0.02±0.07‰ vs. CDT, respectively (all 1σ). Only $\Delta^{33}S$ is statistically different from MORBs, by +0.02‰. The $\Delta^{33}S$ enrichment is invariant across degassing and sulfide segregation. We suggest it reflects a mantle source enrichment rather than a high-temperature fractionation of S in the basalts. Despite the small magnitude of the ^{33}S-^{36}S variations, our data require a substantial amount of recycled sulfur overwhelm the Pitcairn mantle source. We show that models involving metasomatized peridotites, lower crust units, or Archean sediments, may be viable, but are restricted to narrow sets of circumstances. Instead, scenarios involving the contribution of Proterozoic marine sediments appear to be the most parsimonious explanation for the EM-1 signature at Pitcairn.

1. Introduction

Ocean Island Basalts (OIB) sample a variety of mantle reservoirs, often deep seated in Earth's mantle (Weis et al., 2011). Erupted basalts at volcanic islands and seamounts originate from the partial melting of upwelled mantle sources, and reveal a complex history of the deep mantle. The isotopic compositions of basalts show that OIB mantle sources incorporate both primordial noble gases (Mukhopadhyay, 2012; Mukhopadhyay and Parai, 2019; Parai et al., 2019) as well as lithophile elements that are evidently recycled from Earth's surface (Weis et al., 2011; Willbold and Stracke, 2006).

Pitcairn is an island in the South-Pacific ocean, with basalts that host

49 moderately primordial neon (Honda and Woodhead, 2005) associated with a
50 notoriously radiogenic $^{87}Sr/^{86}Sr$ and $^{208}Pb/^{204}Pb$ signature, at some of the least
51 radiogenic $^{206}Pb/^{204}Pb$ (Woodhead and Devey, 1993). This signature is coined
52 Enriched Mantle 1 (EM-1) and likely results from recycling crustal components
53 into a mantle source (Zindler and Hart, 1986). The EM-1 signature requires a low
54 time-integrated $^{238}U/^{204}Pb$ associated with high time-integrated $^{87}Rb/^{86}Sr$ and
55 $^{234}Th/^{238}U$. Various crustal materials have been proposed as the recycled material,
56 including but not limited to a metasomatized lithospheric mantle, oceanic
57 sediments, and components from the lower continental crust (Chauvel et al., 1992;
58 Eisele et al., 2002; Gibson et al., 2005; Turner et al., 2017; Willbold and Stracke,
59 2006; Woodhead et al., 1993).

60 Sulfur isotope signatures may place constraints on the type of material
61 recycled into the Pitcairn mantle plume. Ion probe measurements on sulfide
62 inclusions in olivine, plagioclase, and the matrix from submarine pillow interiors
63 (Delavault et al., 2016) show negative ^{33}S anomalies, down to -0.85±0.25‰. This
64 requires surface-derived sulfur of Archean age is hosted within the Pitcairn
65 mantle source (Delavault et al., 2016). The available ion-probe dataset however
66 lacks ^{36}S measurements. Given that Archean sediments have unique ^{33}S-^{36}S
67 relationships compared to Proterozoic rocks (Farquhar et al., 2007; Johnston,
68 2011), determining $\Delta^{36}S$ would allow testing relative age difference among
69 various recycled materials in the mantle. In order to better constrain the origin of
70 sulfur in the Pitcairn source, we use gaseous source mass spectrometry in dual
71 inlet mode and document high-precision $\delta^{34}S$, $\Delta^{33}S$ and importantly $\Delta^{36}S$
72 signatures of Pitcairn basalts. We evaluate whether crustal, peridotite and/or

sedimentary components contribute to the EM-1 mantle source erupted at Pitcairn.

2. Samples

The Pitcairn hotspot is located in the south Pacific, on oceanic crust that is approximately 25 million years old. Active submarine volcanoes are located about 80 km east of the island of Pitcairn (Hekinian et al., 2003). The active seamounts offer fresh basaltic glassy material that may host geochemical characteristics of the hotspot. Our Pitcairn samples are fresh glasses from the Polynaut cruise (1999). We analyzed glassy rims of pillow basalts sampled with the *Nautile* submersible from the flanks of Bounty, Adam and "volcano 5", at various depths between 3,100 and 1,000 meters below seawater level (Hekinian et al., 2003).

3. Methods

Sulfur was extracted for isotopic analysis via wet chemistry (Labidi et al., 2012). Briefly, centimeter size pieces of glassy basalts were chosen, cleaned and crushed to a grain size < 63 microns. The samples were digested in 20 mL of 2.1 M $CrCl_2$ solution with 5 ml of 12 M HCl and 5 ml of 29 M HF in a Teflon vessel under continuous flushing of pure N_2. Reduced sulfur was extracted as H_2S, bubbled through a water trap and subsequently into a sulfide trap filled with $AgNO_3$ (0.3 M) where H_2S reacted to precipitate Ag_2S. Sulfate occurrence was anticipated as sulfate is often observed in OIB (Jugo et al. 2010). Here, bulk sulfur concentrations are estimated with an electron microprobe, while reduced sulfur is quantified

with our wet chemistry protocol (Labidi et al., 2012). Any sulfates potentially present in glasses remained in the digestion solution (Labidi et al. 2012). We infer the S^{2-}/S_{tot} ratios by mass balance, with a relative uncertainty of ~10%.

The sulfur isotope measurements were performed using a dual inlet MAT 253 gas-source mass spectrometer. Once $\delta^{n}S$ are determined (n = 33, 34, 36), $\Delta^{33}S$ and $\Delta^{36}S$ are calculated ($\Delta^{33}S = \delta^{33}S - 1000((\delta^{34}S/1000 + 1)^{0.515} - 1)$ and $\Delta^{36}S = \delta^{36}S - 1000((\delta^{34}S/1000 + 1)^{1.90} - 1)$). Aliquots of Canyon Diablo Troilite (CDT) analyzed relative to the IPGP reference gas give average $\Delta^{33}S$ and $\Delta^{36}S$ values of -0.024±0.004‰ and −0.13±0.04‰ (1σ, n=11). Repeated analyses of IAEA-S1 versus the IPGP in-house SF_6 tank give $\Delta^{33}S$ = +0.082±0.004‰, $\Delta^{36}S$ = −0.91±0.11‰ (all 1σ, n=43, $\delta^{34}S_{S1}$ is fixed at -0.30‰ and hereafter defines the V-CDT scale). In the following, all $\delta^{34}S$ are reported against V-CDT and all $\Delta^{33}S$ and $\Delta^{36}S$ values are anchored on the CDT scale. Ten of the basalts had their S isotope measurement replicated (supplementary table 1). Most duplicates had $\delta^{34}S$, $\Delta^{33}S$ and $\Delta^{36}S$ values indistinguishable within ~ 0.1, 0.012, and 0.1‰ respectively (1σ), similar to the uncertainty obtained on basalt standards (Labidi et al., 2012). The average value for replicates is given in Table 1, and raw data can be found in the supplementary online file.

More details on the characterization of the glasses can be found in the supplementary material. Briefly, major element, sulfur, copper and chlorine abundance analyses of the glasses were performed using electron microprobe (EMP) techniques on polished sections using a Cameca SX100 at the CAMPARIS facility (Sorbonne Université, Pierre et Marie Curie Campus) under standard conditions described elsewhere (e.g., Labidi et al., 2012). Water concentrations

were quantified on a vacuum line as detailed elsewhere (Clog et al., 2013, 2012). The Sr-Nd-Pb isotope ratios on a selection of Pitcairn glasses were acquired following standard techniques in the Magma-Ocean laboratory, Brest, France, following a published protocol (Mougel et al., 2014).

4. Results

4.1 Major elements

Samples from Adam and Bounty seamounts have MgO contents between 4.5 and 6.0 wt% except for PN14-04 that has an MgO concentration of 2.6 wt% (Fig. 1). Three samples from Volcano 5 show MgO content of ~2.5 wt%. Concentrations in FeO are nearly constant at variable MgO (Fig. 1a), reflecting Fe oxides on the liquid line of descent. We also observe near-constant Al_2O_3 concentrations of ~15 wt% across varying MgO (Table 1, Fig. Supp 1), indicating the suppression of plagioclase crystallization. These two observations are consistent with a calc-alkaline differentiation trend (Zimmer et al., 2010). All samples have high concentrations of incompatible major elements. The K_2O content is > 0.8 wt% (up to 2.8 wt%), and Na_2O concentrations are > 3.5% for most samples (Table 1). High concentrations of K_2O and Na_2O are characteristics of alkali basalts and reflect low partial melting fractions, below < 8% (Aubaud et al., 2006; Hekinian et al., 2003) as well as crystal fractionation. High K_2O/TiO_2 ratios of ~ 0.4 are observed for samples with MgO > 4 wt%. (Fig. 1b). High K_2O/TiO_2 likely represent a mantle source enrichment associated with the Pitcairn hotspot (Jackson and Dasgupta, 2008). For samples with MgO < 4 wt%, K_2O/TiO_2 are even higher, likely reflecting the late onset of titanomagnetite precipitation at MgO ~

4% which causes TiO_2 fractionation and hence increases even further the K_2O/TiO_2 ratios.

4.2 Volatile and supporting minor elements in Pitcairn basalts

We report chlorine contents of < 800 ppm for all Pitcairn lavas (Table 1). Combined with K_2O abundances determined here, Cl/K ratios are < 0.05 for Bounty, <0.04 for Adam, and <0.02 for volcano 5 (Table 1). Water contents range between 5,700 and 12,100 ppm. The average H_2O content is 8304±1983 ppm (1σ). The observed H_2O concentrations are typical of OIB (Dixon et al., 2002; Workman et al., 2006) and overall higher than MORB (Clog et al., 2013; Michael, 1995; Sobolev and Chaussidon, 1996).

In Bounty lavas, bulk S contents vary between 512±50 and 1416±50 ppm S (Fig. 2). Among Bounty lavas, samples from dive 3 have homogeneous major element compositions, but display most of the S content variability, with values ranging from 738±50 to 1416±50 ppm S (Table 1). The glasses collected from dive 3 also have S contents that are correlated with eruption depth (Fig. 3). At Adam, two glasses show S contents of 799±50 and 762±50 ppm S. At Volcano 5, two glasses show S contents of 573±50 and 602±50 ppm S.

The S^{2-}/S_{tot} ratios of 12 out of the 15 Pitcairn lavas are within uncertainty of 1, indicating a small amount (if any) of dissolved sulfate. Three other lavas, all from Bounty, picked in the dive 3, show S^{2-}/S_{tot} ratios of 0.76±0.04, indicating measurable sulfate abundances. No correlations appear between S^{2-}/S_{tot} ratios and bulk S content, or between S^{2-}/S_{tot} ratios and eruption depths.

In lavas with MgO > 4 wt%, Cu contents range between 60±10 and 33±10

ppm Cu (Fig. 4). For the more evolved bounty sample (PN14-04) and lavas from volcano 5 (PN08-01 and 08-07), Cu contents are below 10 ppm.

4.3 Sulfur isotopes ratios

Sulfur isotope ratios are given here as $\delta^{34}S$, $\Delta^{33}S$, and $\Delta^{36}S$ values for reduced S, which for most samples correspond to bulk sulfur (Fig. 5A). The $\delta^{34}S$ values range between -1.3‰ and +1.6‰, averaging at -0.4±1.0‰ (n=15). For Bounty, $\delta^{34}S$ values vary between -1.3‰ and +0.7‰, with an average of -0.7±0.7‰. The 2 samples from Adam have $\delta^{34}S$ values of -1.2‰ and -1.1‰. For volcano 5, the two glasses both have $\delta^{34}S$ values of +1.6‰. As shown on figure 5B, our $\delta^{34}S$ values do not duplicate the largely negative $\delta^{34}S$ values on individual sulfide inclusions from Bounty pillow lavas obtained by ion probe measurements (Delavault et al., 2016).

Reduced sulfur displays rather homogenous $\Delta^{33}S$ and $\Delta^{36}S$ among all basalts (Fig. 5A and Fig. 6). $\Delta^{33}S$ and $\Delta^{36}S$ averages are +0.023±0.007‰ and +0.02±0.07‰ vs. CDT, respectively (1 s.d.). Our $\Delta^{33}S$ data are inconsistent with the substantially negative $\Delta^{33}S$ ion probe estimates on individual sulfide inclusions (Delavault et al., 2016). For the dive 3 at Bounty, the $\Delta^{33}S$ and $\Delta^{36}S$ average values are +0.026±0.004‰ and +0.07±0.04‰ (1 s.d.). The $\Delta^{36}S$ values at Pitcairn extend to values that are somewhat higher than MORB estimates of -0.04+±0.08, (1 s.d.) (Labidi and Cartigny, 2016) but average values remain similar within the 1σ level. The $\Delta^{33}S$ average of +0.023±0.007‰ is distinctly higher than MORB average of +0.007±0.006‰ (1 s.d., Labidi and Cartigny, 2016) at both 1 and 2σ confidence level. We note that the sample PN14-04, from Bounty, has a MORB-like $\Delta^{33}S$ value.

Should it be excluded, the $\Delta^{33}S$ average at Pitcairn would become 0.024±0.006‰.

Simple t-tests on both $\Delta^{33}S$ and $\Delta^{36}S$ values would suggest a significant difference between Pitcairn and MORB may exist, but would not take into account analytical error. We use a Monte-Carlo approach to evaluate whether the differences in the averages are statistically significant and consider analytical uncertainties. We generate simulated datasets for the MORB and Pitcairn samples, based on sampling a normal distribution for each sample with an average equal to the measured value and a standard deviation equal to the corresponding analytical uncertainty. We then run a Welch's t-test and repeat the process 10,000 times. Histograms and kernel density plots are shown in Fig. 7. For ^{36}S, Pitcairn melts show an average value significantly distinct ($p < 0.05$) from MORBs only in 40% of the simulations. Thus, we suggest MORB and Pitcairn $\Delta^{36}S$ are not significantly different. In contrast, the means of the $\Delta^{33}S$ values are significantly distinct ($p<0.05$) in 99.9% of the simulation runs, confirming the $\Delta^{33}S$ enrichment at Pitcairn is statistically significant.

4.4 Radiogenic isotopes

We analyzed the Sr-Pb-Nd isotopic composition with a focus on the samples from the dive 03, from the Bounty seamount, which has the least differentiated basalts. For all samples but PN14-04, the $^{87}Sr/^{86}Sr$, $^{143}Nd/^{144}Nd$ and $^{206}Pb/^{204}Pb$ ratios are homogeneous, with values ranging between 0.704466 and 0.704624, 0.512537 and 0.512944, and 17.74 and 17.92, respectively (Fig. Supp 3). We observe relatively high $^{208}Pb/^{204}Pb$ and $^{207}Pb/^{204}Pb$ ratios at a given $^{206}Pb/^{204}Pb$. The radiogenic isotope data are in agreement with previous work performed on

215 the same glasses (Bourdon and Van Orman, 2009), or on different samples from
216 Pitcairn (Woodhead et al., 1993, Delavault et al, 2016). For almost all samples, the
217 data is consistent with an extreme EM-1 endmember. Only PN14-04, from Bounty,
218 has a $^{206}Pb/^{204}Pb$ higher than 18.0 and a $^{87}Sr/^{86}Sr$ lower than 0.7041 (see below).
219 This illustrates a slightly distinct mantle source, somewhat less affected by the
220 EM-1 signature.

221

222 **5. Discussion**

223 The lavas studied here underwent a complex history prior to eruption. This
224 involves mantle source enrichment with an EM-1 component, low partial melting,
225 magmatic differentiation following a calc-alkaline trend, and various amounts of
226 volatile losses via degassing. Below, we constrain the magmatic behavior of sulfur
227 in our samples and identify the respective contributions of sulfide fractionation
228 and sulfur degassing. Ultimately, we estimate the sulfur isotope composition of the
229 mantle source for $\delta^{34}S$, $\Delta^{33}S$, and $\Delta^{36}S$ signatures.

230 **5.1 Limited crustal assimilation**

231 Hydrothermal brine assimilation may be sporadically associated with
232 contamination by hydrothermal sulfides (Labidi et al., 2014). Cl and K have a
233 similar incompatible behavior during mantle melting and basalt differentiation
234 (Michael and Cornell, 1998; Michael and Schilling, 1989). However, Cl is enriched
235 in the hydrated oceanic crust and in brines. Thus, elevated Cl/K ratios in basalts
236 are treated as evidence for crustal assimilation. Here, the Cl/K are < 0.05 for
237 Bounty, <0.04 for Adam, and <0.02 for volcano 5 (Table 1). The Cl/K for the three

238 localities are below the threshold of 0.1, above which lavas are argued to undergo
239 contamination by Cl-rich brines (Michael and Cornell 1998). We conclude our
240 samples unlikely assimilated hydrothermal components prior to eruption, and
241 thus we assume their S isotope composition has remained unaffected by
242 potentially contaminant sulfides from the crust.

243

244 **5.2. Sulfide saturation in Pitcairn melts**

245 Pitcairn lavas have MgO < 6 wt% (Fig. 1), indicative of substantial crystal
246 fractionation, with near-constant FeO concentrations of ~9.5% across the range
247 in MgO (Fig. 1). In tholeiitic basalts, FeO concentration is the prime factor
248 controlling sulfur content at sulfide saturation (Mathez, 1976). If this relationship
249 is at all maintained in calc-alkaline melts, one would anticipate invariable S
250 concentrations at a particular value defined by the sulfur solubility at sulfide
251 saturation. These are, however, not observed: we observe variation of S
252 concentrations over almost a factor of 3 at a given FeO (or MgO) content (Fig. 2).
253 Sulfide fractionation could explain the dramatic variation in sulfur
254 concentration in Pitcairn melts (Fig. 2). Although challenging to quantify (Jenner
255 et al., 2010; Yierpan et al., 2019), sulfide fractionation may be singled out via the
256 copper systematics : the partition coefficient of Cu is ~10^{-1} and ~10^{3} for
257 crystal/melt and sulfide/melt, respectively (Lee et al., 2012). Thus, in the absence
258 of sulfides on the liquidus, copper behaves as a moderately incompatible element
259 and increases with decreasing MgO, as observed in arc-magmas and other OIB.
260 Once sulfide saturation is met, Cu abundances drop as copper is readily
261 partitioned into sulfides (Lee et al., 2012, Labidi et al., 2015). This behavior of Cu

is not observed at Pitcairn. Here, Cu concentrations appear coincidentally similar to MORBs, with a near-constant Cu concentration across most of the MgO range (Fig. 4). The data appear more consistent with a liquid line of descent that is typical of MORB, where a roughly constant rate of sulfide fractionation occurs during magmatic differentiation range (Labidi et al., 2014). We thus argue that while sulfides existed on the liquidus of Pitcairn melts, dramatic sulfide fractionation is not the cause of varying S concentration at a given FeO, observed on Fig. 2.

5.3. Magmatic degassing

Sulfur degassing could account for the variable sulfur concentrations observed on Fig. 2. We focus on samples from the dive 3 from Bounty, because these lavas are comparable in terms of major elements and radiogenic isotope compositions (Table 1), so their sulfur concentrations prior to eruption can be assumed at zero-order to be homogeneous. Basalts from the dive 3 however were erupted at various depths on the flank of the volcano (Hekinian et al., 2003). Dissolved sulfide (S^{2-}) abundances range from 1300±50 ppm to 550±50 ppm and are correlated with the depth of eruption: the shallowest samples have the lowest S concentrations (Fig. 3). We interpret this relationship as evidence for sulfur degassing upon eruption. We quantify the residual sulfur fraction *f* as the ratio of the observed S concentration to the highest S concentration observed here, ~1300 ppm S. For S concentrations between 1300±50 ppm and 550±50 ppm S, we infer *f* values are between 1 and 0.45. Note that the starting S concentration could be

285 even higher than ~1300 ppm, but this does not fundamentally change our results
286 below.

287 Sulfur degassing is consistent with water behavior in our melts. Across
288 decreasing depths, the H_2O abundances decrease from ~9500±500 ppm to
289 5500±500 ppm water (Fig 3). The H_2O/K_2O range between 0.69 and 0.35 (Table
290 1), decreasing by a factor of ~2 across the depth rise (Fig 3). Water and potassium
291 oxide have comparable incompatible behaviors (Danyushevsky, 2001; Michael,
292 1995) and may not be substantially fractionated from each other by crystal
293 fractionation. Instead, observed decreasing H_2O/K_2O at increasingly shallow
294 eruption depths is compatible with H_2O degassing. Importantly, sulfur
295 concentrations are correlated with H_2O/K_2O ratios (Supp Fig. 4). The simplest
296 explanation involves the concomitant degassing of water and the reduced fraction
297 of sulfur from the melts during eruption. We note that the concomitant degassing
298 of reduced S and water during eruption is not unique to Bounty. A similar
299 degassing trend featuring sulfur and water was observed in Hawaii basalts
300 (Brounce et al., 2017; Dixon et al., 1991).

301

302 **5.4. Interpreting $^{34}S/^{32}S$ ratios in Pitcairn glasses**

303 The $\delta^{34}S$ values of reduced S from all Pitcairn basalts analyzed here range
304 between -1.3‰ to +1.6‰. At Bounty, values are between -1.3‰ and +0.7‰.
305 Bounty basalts from the dive 3 have homogeneous Cu concentrations at a given
306 MgO content, suggesting they underwent comparable amounts of immiscible
307 sulfide losses (Table 1). Isotope fractionation during sulfide segregation is

308 therefore discarded to explain the variable $\delta^{34}S$ values seen in basalts from the
309 dive 3. In figure 8, we plot $\delta^{34}S$ values against *f* values calculated for samples from
310 the dive 3. $\delta^{34}S$ appear increasingly negative at lower *f* and may be interpreted in
311 terms of isotopic fractionation associated with degassing under open-system
312 distillation (Fig. 8A). One possibility involves two starting endmember
313 compositions, with two steep trends. To cause the decrease in $\delta^{34}S$ in the residual
314 melt, the vapor phase must preferentially partition heavy ^{34}S isotopes, under a
315 bulk isotope fractionation of 2‰ ($\alpha_{gas\text{-}melt}$ = 1.002). This happens to be
316 indistinguishable from predicted SO_2-S^{2-} isotopic fractionation at equilibrium at
317 1,200 °C (Mandeville et al. 2009). This average melt-gas isotope fractionation
318 would suggest SO_2 is the dominant S-bearing species during equilibrium
319 degassing. A similar suggestion was made for basalts from the Canary Islands
320 (Beaudry et al., 2018). It is unclear whether equilibrium SO_2 degassing could also
321 offer a possible explanation for the low $\delta^{34}S$ observed in sulfides from Pitcairn
322 pillows (Delavault et al., 2016) as they do not report S concentrations of the
323 basalts they analyzed. The eruption of depths of the Bounty basalts studied by
324 Delavault et al., (2016) is ~1,000 meters, substantially shallower than our samples,
325 consistent with a pattern of more pronounced SO_2 degassing.

326 A caveat in our degassing interpretation comes from observation of
327 variable $\delta^{34}S$ at a given *f*, on Fig. 8. This inevitably requires multiple starting
328 compositions. The scenario of equilibrium SO_2 degassing requires two starting
329 compositions of ~-0.7 and ~+0.2‰ (Fig. 8) for $\delta^{34}S$. The data may alternatively
330 be interpreted as degassing under much smaller isotope fractionations. Most
331 basalts have $\delta^{34}S$ compositions that can be explained as the result of S degassing

under a near-zero gas-melt isotope fractionation of -0.1‰ ($\alpha_{gas\text{-}melt}$ = 1.0001), with a starting $\delta^{34}S$ of –0.9‰, indistinguishable from the Pacific MORB mantle (Labidi et al., 2014), as illustrated on Fig. 8B. The degassing fractionation is consistent with S^{2-}—H_2S isotopic fractionation at equilibrium (Beaudry et al., 2018, Mandeville et al. 2009). However, when three glasses with high $\delta^{34}S$ at a given *f* are included, this degassing scenario suggests no less than three initial starting compositions. In summary, the data appear to inevitably argue in favor of multiple starting $\delta^{34}S$ compositions for the Bounty melts, spread over ~1‰ above the MORB estimates and our isotope data alone may not unambiguously disambiguate H_2S and SO_2 degassing scenarios.

5.5. The recycled component at Pitcairn mantle sources

The parental melts at Pitcairn show a $\delta^{34}S$ range, restricted between –1‰ and +0.5‰ (Fig. 8). Our $\delta^{34}S$ estimate points to values above the MORB range, for basalts with EM-1 signatures. In consideration of the vulnerability of our degassing scenarios (section 5.4), and the uncertainty associated with estimated starting compositions, we are unable to interpret all $\delta^{34}S$ data as a straightforward representation of source composition. In the following, we focus on $\Delta^{36}S$-$\Delta^{33}S$ data which remain unmodified by degassing, as attested by a lack of correlation between on $\Delta^{36}S$-$\Delta^{33}S$ and *f* values (Table 1). Our $\Delta^{36}S$ and $\Delta^{33}S$ are homogeneous (with one outlier with a MORB-like $\Delta^{33}S$ signature, PN14-04), but the average $\Delta^{33}S$ is statistically distinct from MORB (Fig. 5, 7). Pitcairn samples show a small positive $\Delta^{33}S$ anomaly of ~0.02‰. We attribute the small-magnitude $\Delta^{33}S$ enrichment to subducted sulfur, associated with the recycled component responsible for the EM-1 Pitcairn signatures. Our $\Delta^{33}S$ values, duplicated for most

356 basalts (supplementary table 1), are not consistent with large negative $\Delta^{33}S$
357 anomalies reported elsewhere via ion probe measurements on individual sulfides
358 from Bounty basalts (Delavault et al., 2016). In the following, we provide
359 interpretations for our dataset and briefly discuss if our data may be reconciled
360 with suggestions made in Delavault et al., (2016).

361 We plot our $\Delta^{36}S$-$\Delta^{33}S$ data on Fig. 9, together with a compilation of
362 sediments from the literature (Johnston, 2011). The plot shows the difference
363 between Archean components, with $\Delta^{36}S/\Delta^{33}S \sim -1$, and post-Archean rocks, with
364 $\Delta^{36}S/\Delta^{33}S \sim -7$ (Farquhar et al., 2007). Post-Archean rocks show a much smaller
365 $\Delta^{33}S$ range than Archean sediments. We posit that the recycled endmember at
366 Pitcairn falls within the existing fields defined by literature data on surface rocks
367 shown on Fig. 9. Our approach relies on the assumption that no systematic $\Delta^{33}S$–
368 $\Delta^{36}S$ isotope fractionation may be associated with metamorphism and slab
369 devolatilization (Dottin III et al., 2020a). We examine various mixing scenarios. In
370 all, we discuss the prospect of two-component mixing between a mantle peridotite
371 with a recycled component. A mass balance is considered successful if can fit the
372 observed $\Delta^{33}S$–$\Delta^{36}S$ compositions at Pitcairn with a reasonable set of restrictions.

373 The Pitcairn $\Delta^{33}S$ enrichment is associated with a near-invariant, MORB-
374 like $\Delta^{36}S$ signature (Fig. 5–7). For recycled sulfur to be of Proterozoic age and plot
375 within the field defined by published sedimentary data (Fig. 9), the $\Delta^{33}S$ signature
376 of the Pitcairn endmember is allowed to be between ~0.03 and ~ 0.10‰ with a
377 $\Delta^{36}S$ between ~ -0.4 and ~ 0.4‰ ('plausible Pitcairn endmember' on Fig. 9A). This
378 is well within the $\Delta^{33}S$ range in the Proterozoic of ~0.20‰ (Fig. 9). This is also

consistent with the frequent near-zero $\Delta^{36}S$ at a varying $\Delta^{33}S$ observed in the geological record, especially when sedimentary sulfates are considered (Fig. 9A). Archean signatures are far more variable in $\Delta^{33}S$, such that a 0.020‰ ^{33}S enrichment at Pitcairn is minuscule compared to most Archean anomalies (Fig. 9B). The Pitcairn endmember could be a diluted Archean signature, which would happen to mimic the magnitude of Proterozoic sediment. In this case, our observation of an invariant $\Delta^{36}S$ requires the Archean signature to have a $\Delta^{36}S$ between ~ -0.4 and ~ 0.4‰. Positive $\Delta^{33}S$ at near-zero $\Delta^{36}S$ exist in the Archean, if $\Delta^{33}S$ remains in a restricted range between 0.1 and ~1.0‰ ('plausible Pitcairn endmember' Fig. 9B). This exercise illustrates that although the magnitude of Proterozoic sediments appears more consistent with the Pitcairn ^{33}S data than Archean rocks, both Archean and Proterozoic components could theoretically account for the signatures at Pitcairn. However, Archean signatures have implications that may be harder to reconcile with the geological record. This is detailed below in the context of the various geochemical models that account for the nature of EM-1.

5.5.1 The metasomatism hypotheses for EM-1 at Pitcairn

Delamination of lithospheric mantle has been suggested to yield EM-1 signatures. This is an umbrella concept, involving either sub-oceanic or sub-continental depleted peridotites. The peridotites would develop EM signatures after experiencing metasomatism by either low-degree silicate melts or by slab-derived fluids (Hart et al., 1986; McKenzie and O'nions, 1983). One suggestion is that EM-1 originates from the Sub-Continental Lithospheric Mantle (SCLM), after it experienced metasomatism by melts from the asthenosphere (Hoernle et al.,

403 2011; McKenzie and O'Nions, 1995). This mechanism was found to generate EM-
404 1 components in convergent margins, where it is clear that no contributions
405 occurred from subducted components (Turner et al., 2017). In light of this
406 hypothesis, we anticipate a scenario in which low-degree melts from the
407 asthenosphere would deliver sulfur with MORB-like $\Delta^{33}S$ of ~0.007±0.006‰
408 (Labidi and Cartigny, 2016), in conflict with the $\Delta^{33}S$ excess in the Pitcairn basalts.
409 The SCLM may alternatively experience metasomatism by subduction fluids.
410 Gibson et al. (2005) and Meyzen et al., (2005) reviewed evidence for peridotites
411 metasomatized by subduction fluids, and showed they are dominated by EM-2
412 signatures, but EM-1 compositions are also observed. This metasomatized
413 component could for instance contribute to the EM-1 Tristan mantle source at
414 about ~10% (Gibson et al., 2005). A similar scenario was suggested for Pitcairn,
415 on account of the absence of oxygen isotope variations in basalts associated with
416 extreme EM-1 compositions (Eiler et al., 1995, 1997). This idea has the advantage
417 of offering a mechanism to deliver surface-derived S (thus showing variable ^{33}S
418 signatures) inherited from either sediments or the altered oceanic crust, to a
419 lithospheric unit. We consider the sulfur isotope consequences of such a two-
420 component mixing, assuming a contribution of metasomatized peridotites of ~
421 10% (Gibson et al., 2005) mixed with 90% of a deep mantle source showing a
422 MORB-like $\Delta^{33}S$ (Dottin III et al., 2020b) and 200 ppm S concentration (Lorand
423 and Luguet, 2016; Nielsen et al., 2014). The metasomatized peridotites are
424 assigned the entirety of the $\Delta^{33}S$ anomaly, and S concentrations between 50 and
425 400 ppm S, as observed in natural samples (Lorand and Luguet, 2016). These
426 endmember concentrations reflect how much a SCLM experiences sulfur
427 depletion by partial melting prior to being metasomatized (Lorand and Luguet,

2016). There are no constraints on which endmember scenario may be more relevant for Pitcairn, and therefore we explore the two possibilities with no *a priori* estimate on how they may remain viable for other trace elements. Taking 400 ppm for [S], the 10%-90% two-component mixing requires the SCLM to show an average $\Delta^{33}S$ of ~0.09‰ to account for the ~0.02‰ enrichment at Pitcairn. Taking 50 ppm S, the required $\Delta^{33}S$ value becomes ~0.55‰. This illustrates that again, both Archean and post-Archean sulfur could explain the data in the SCLM scenario.

Scenarios requiring melt depletion followed by fluid-driven enrichments are not supported by trace element signatures at Pitcairn. Notably, systematic enrichments or depletions of fluid mobile elements are not observed in the Pitcairn source (e.g. Nb anomalies, Willbold and Stracke, 2006). The integrated dataset therefore does not argue in favor of a scenario involving a subduction-imprinted SCLM in the Pitcairn source.

5.5.2 The effect of incorporating Lower Continent Crust

Delamination of the lower continental crust (LCC) could be a viable alternative to account for EM-1 signatures in plumes (Willbold and Stracke, 2006). Meyzen et al., (2005) showed granulites from the lower continental crust develop signatures far closer to EM-1 than samples from the SCLM. Only ~2% of LCC is necessary to contribute to any mantle source to generate the Pitcairn EM-1 signature (Willbold and Stracke, 2006). In addition, the somewhat variable trace element signature of various LCC units offers an explanation for the irregular trace element patterns among EM-1 hotspots (Willbold and Stracke, 2006).

We consider the sulfur isotope consequences of a two-component mixing scenario where the LCC contributes 2% of the bulk mass of the Pitcairn source

453 (Willbold and Stracke, 2006). Assuming a concentration of 350 ppm S in the LCC
454 (Rudnick et al., 2003), mass balance requires the average LCC to show a $\Delta^{33}S$ of
455 ~0.7‰ to account for the ~0.020‰ ^{33}S excess observed in the Pitcairn source.
456 This would put the LCC unit in the Archean domain (Fig. 9B).

457 The LCC reservoir is severely under-constrained, with a ^{33}S isotope
458 composition remaining virtually unknown. Mafic granulites essentially carry
459 igneous sulfur, with a MORB-like $\delta^{34}S$ signature (Wedepohl, 1995), consistent
460 with the common idea that they result from crustal underplating by
461 asthenosphere melts (Rudnick et al., , 2003). If so, the lower crust would have
462 MORB-like $\Delta^{33}S$-$\Delta^{36}S$ signatures. This would render the LCC unable to account for
463 the ^{33}S isotope anomaly that characterize the Pitcairn source. Felsic granulites also
464 exist in the lower crust. They apparently show non-mantle $\delta^{34}S$ signatures,
465 illustrated by a modest ^{34}S enrichment of ~3‰ (Wedepohl, 1995). A complex
466 model where delaminated felsic granulites would happen to have a $\Delta^{33}S$ of ~0.7‰,
467 inherited from Archean rocks, could be invoked to account for the data at Pitcairn.
468 However, it would be inconsistent with the few available data on Archean crustal
469 melts, with near-zero $\Delta^{33}S$ values (Bucholz et al., 2020). We cannot exclude that at
470 an unconstrained location and time, an analogous process in a hypothetical LCC
471 resulted in felsic components with a high $\Delta^{33}S$ average value of exactly 0.7‰, but
472 this scenario appears restrictive and speculative.
473
474 **5.5.3 A sedimentary origin: Archean exhalates in Pitcairn?**
475 SIMS measurements on sulfides from other Pitcairn lavas from Bounty
476 (Delavault et al., 2016) yielded $\Delta^{33}S$ values down to ~-0.85±0.25‰. The

substantial ^{33}S anomaly was attributed to the contribution of Archean exhalates, an uncommon type of Archean chemical sediments that so far were only observed in the Abitibi greenstone belt (Delavault et al., 2016). Our high-precision $\Delta^{33}S$-$\Delta^{36}S$ data do not reproduce the large negative $\Delta^{33}S$ anomalies observed by Delavault et al., (2016). Instead, the data establish the Pitcairn source to have positive ^{33}S anomalies, at odds with Archean exhalates. Furthermore, although exhalates may be enriched in trace elements, their rare earth patterns do not match any reconstructed slab component contributing to the Pitcairn mantle source (Delavault et al., 2016). Thus, ad-hoc modification during subduction (e.g., fluid losses causing trace element fractionation) was invoked to account for the EM-1 trace element data (Delavault et al., 2016). Again however, the Pitcairn trace element compositions lack the typical fluid-loss signatures like Nb anomalies (Willbold and Stracke, 2006). Up to about ~20% of a component resulting from the processing of the exhalates was suggested in the Pitcairn mantle source (Delavault et al., 2016). It is unclear whether this may be reconcilable with a mantle source suggested to be almost exclusively dominated by peridotites (Jackson and Dasgupta, 2008), perhaps with a minor pyroxenitic component (Nebel et al., 2019). It also appears to conflict with the absence of O isotope anomalies in Pitcairn basalts, that would likely be observed for any sediment contribution higher than 2% (Eiler et al., 1995). As it stands, although the S isotope compositions measured by Delavault et al. suggest a contribution from Archean exhalates, the majority of geochemical data published on Pitcairn basalts suggests otherwise.

5.5.4 The return of conventional marine sediments

Invoking the subduction of marine sediments has been a classic scenario in

chemical geodynamics (Hofmann and White, 1982). As for the SCLM or the LCC scenarios, sediment recycling is a viable hypothesis that requires a specific mixing ratio. Here, we assume a 2% contribution of sediment into Pitcairn source (Eisele et al., 2002). Note that variations between 1 and 4%, in the range of reasonable predictions for EM signatures (Jackson and Dasgupta, 2008), would yield comparable results.

From our data we can establish a first-order mass balance scenario from the standpoint of S concentrations. Taking 2% contribution of sediment into a 98% peridotite source, and S concentrations in the sediments ranging between 2,500 and 10,000 ppm S, sediments with $\Delta^{33}S$ of +0.10‰ and +0.025‰ would result in mixtures with $\Delta^{33}S$ ~0.02‰. This would match our ^{33}S observations in basalts. Should the sediments also show a $\Delta^{36}S$ between ~ -0.4 and ~ 0.4‰ as illustrated in Fig. 9A, the ^{36}S data in basalts would also be accounted for. The concentrations between 2,500 and 10,000 ppm, required by the mass balance, are in the wide range shown by Proterozoic sediments showing typically between 100 and 30,000 ppm S (Poulton et al., 2004). This simple mass balance calculation shows that Proterozoic sediments with moderate S concentrations may contribute to the Pitcairn source for the S isotope basalt data to be accounted for. Concluding on whether or not the required S concentrations are significantly low compared to non-subducted sediments, perhaps because of sulfur losses during subduction, appears unwarranted. However, we note that the mass balance exercise does not require having to generate any hypotheses on the sulfur behavior in ancient subduction zones. Considering how contentious the notion of sulfur losses in subduction is, even for well-studied subduction zones in the Phanerozoic (Li et al., 2020, Walters et al., 2020), the lack of strict restrictions of our mass balance with

regard to sulfur behavior in subduction is noteworthy.

In a similar exercise for Archean sediments, we find the maximum plausible $\Delta^{33}S$ of ~1‰ for recycled S, as required by the invariant $\Delta^{36}S$ and the field of Archean signatures (Fig. 9B). For a $\Delta^{33}S$ between +0.2‰ and +1‰, the S concentration of the recycled component is between ~1000 and ~200 ppm, respectively. These concentrations exist in the Archean record, but remain uncommon: >99% of Archean sediments have S concentrations between 500 and 20,000 ppm S (Reinhard et al., 2013). The simple mass balance shows that recycled Archean sediments would be required to have low S concentrations to account for the data in Pitcairn basalts, perhaps indicating a role for sulfur losses during subduction. We cannot rule out this scenario, but we note that it adds a level of restriction compared to the mass balance involving Proterozoic sediments.

To summarize, 2% of marine sediments with variable S concentrations, recycled in the Pitcairn mantle source, could easily explain the S isotope signature of Pitcairn basalts. We find that requiring a Proterozoic age for recycled sediments allows a rather large range of plausible S concentrations, and a tight range of S isotope composition within the post-Archean isotope field (Fig. 9A). The mass balance exercise allows for (but does not require) higher sulfur contents prior to subduction, should sulfur losses be substantial during slab devolatilization. Assuming an Archean age requires the small ^{33}S enrichment at Pitcairn results from the dilution of an Archean component in the Pitcairn mantle source, resulting in an average ^{33}S enrichment resembling in magnitude what is observed in Proterozoic sediments. For a dilution of a putative Archean signature to be achieved, low S concentration in the recycled sediment is required. In other words, this model requires a tight range of S isotope compositions within the known

552 Archean field (Fig. 9B), but also demands a narrow range of sulfur concentrations.
553 Although Archean sediments are not ruled out, the scenario of Proterozoic
554 sediment appears the least restrictive, and therefore the most parsimonious
555 hypothesis to account for the Pitcairn EM-1 signature.
556
557 **5.5.5. Implications on other geochemical signatures**
558 The absence of resolvable ^{18}O isotopes variations in basalts (Eiler et al., 1995,
559 1997) was suggested to argue against sediment recycling in the Pitcairn source.
560 However, the cut-off sensitivity threshold of O isotopes is at ~2% sediment
561 contribution (Eiler et al., 1995). It is conceivable that ≤ 2% sediment may not be
562 detected, even with precise ^{18}O measurements. Another critique of the sediment
563 model came from Willbold and Stracke (2006). Various EM-1 hotspots have
564 irregular trace element patterns, notably in terms of Ba and Rb enrichments
565 (Willbold and Stracke, 2006); Pitcairn is peculiar in that it shows the lowest Ba
566 enrichment of all EM-1 signatures, with Ba/La ratio of ~9 only, much lower than
567 what is seen at Tristan (Ba/La ~17, Willbold and Stracke, 2006). This variability
568 across various EM-1 hotspots is a problem for any unifying model aimed at
569 lumping together all EM-1 compositions as a family of mantle signatures. This was
570 considered evidence against sediment recycling (Willbold and Stracke, 2006),
571 since sediments are thought to have unimodal Ba enrichments (Plank and
572 Langmuir, 1998). The unimodal distribution however does not erase the
573 substantial sedimentary variability for Ba enrichments. In fact, the Ba/La ratios of
574 various sedimentary piles varies greatly, between 8 (MAR 800) and 171 (Central
575 America) (Plank and Langmuir, 1998). Any sediments with a Ba/La < 50, largely
576 in the range of modern sediments (Plank and Langmuir, 1998), would explain the

low Ba/La ratio at Pitcairn. Worldwide EM-1 components with variable Ba/La ratios may simply reflect the natural variability of sedimentary protoliths, as illustrated by modern sediments.

The lead isotope systematics can provide constraints on time-integrated elemental ratios, as well as model ages of recycled components (Chauvel et al., 1992). Delavault et al., (2016) suggested taking μ values ($^{238}U/^{204}Pb$) of ~6 and κ values ($^{232}Th/^{238}U$) of ~7 could yield a model age for the recycled sediment between 2.4 and 2.8 Ga. Here, we suggest relaxing the constraint of an Archean $\Delta^{33}S$ signature. Considering that most sediment columns in modern trenches have μ between ~1 and 13, and κ values between ~1 and 9 (Plank and Langmuir, 1998), we suggest that any combination of $\kappa > 5$ and $\mu < 10$ yields the EM-1 $^{206}Pb/^{204}Pb$, $^{207}Pb/^{204}Pb$ and $^{208}Pb/^{204}Pb$ signatures at Pitcairn with model ages lower than 2 Ga, consistent with a post-Archean $\Delta^{33}S$ signature.

6. Conclusions

We report on 15 submarine alkaline basalts at Pitcairn of EM-1 type. Low copper concentrations suggest all the samples were sulfide saturated upon eruption. The basalts show evidence for sulfur and water degassing, likely causing $\delta^{34}S$ fractionation. Accurately estimating the $\delta^{34}S$ value of undegassed melts is challenging but they are likely between -1 and +0.7‰, higher than the pacific upper mantle estimates of –0.9±0.1‰. The samples have no resolvable ^{36}S variation relative to MORBs. In contrast, reduced sulfur displays homogenous $\Delta^{33}S$, averaging at +0.024±0.006‰ vs. CDT. This is higher than the $\Delta^{33}S$ MORB average

of +0.007±0.006‰, by ~0.015-0.020‰. We attribute the small ^{33}S anomaly to the recycling of surface-derived sulfur in the mantle source of Pitcairn. We show that metasomatized peridotites or components from the lower continental crust, appear inconsistent with the S isotope data, or would require narrow sets of unlikely circumstances. Archean sediments with large positive ^{33}S anomalies could explain the data, but also present tight requirements. The contribution of ~2% Proterozoic sediments in the Pitcairn mantle source represents the simplest explanation, with the lowest amounts of restrictions.

Acknowledgments

JL thanks James Farquhar and Isabelle Genot for comments on an early version of the manuscript. PC acknowledges partial support from the Dear-Sir ANR-15-CE31-005 project of the Agence Nationale de la Recherche. JD acknowledges NSF Postdoctoral Fellowship Award # 2052944. We thank Oliver Nebel and an anonymous reviewer for helpful comments. Rosemary Hickey-Vargas is thanked for editorial handling.

Captions

sample ID	pn02-01	pn02-05	pn03-08	pn03-10	pn03-01	pn03-02	pn03-03	pn03-04	pn03-05	pn03-07	pn03-11	pn14-04	pn14-07	pn08-01	pn08-07
seamount	adam	adam	bounty	bounty	bounty	bounty	bounty	bounty	bounty	bounty	bounty	bounty	bounty	volc. 5	volc. 5
depth (mbsl)	1595	1001	2250	2165	2508	2508	2500	2480	2408	2276	1957	1705	1513	3103	
Na_2O	3.7	3.7	4.2	3.5	4.2	4.2	4.2	3.6	3.8	3.9	4.0	4.2	3.5	4.2	4.2
SiO_2	48.4	48.3	48.8	50.6	47.8	47.9	47.7	49.0	47.8	47.6	48.9	54.2	50.3	54.3	54.4
K_2O	1.5	1.4	1.6	0.8	1.4	1.4	1.5	1.3	1.4	1.4	1.6	2.3	0.9	2.8	2.7
Al_2O_3	15.5	15.5	16.2	15.1	16.0	16.0	15.8	15.8	15.4	15.3	15.3	15.3	15.1	16.2	16.1
CaO	9.0	8.9	8.1	8.6	9.1	9.1	9.1	9.4	9.8	9.7	8.7	5.4	8.6	4.9	4.9
MgO	5.3	6.0	5.0	5.6	5.4	5.5	4.8	5.0	5.2	5.4	4.6	2.6	5.5	2.4	2.6
P_2O_5	0.8	0.8	0.8	0.5	0.7	0.7	0.8	0.7	0.7	0.7	0.8	1.2	0.5	1.3	1.2
FeO	9.8	10.0	9.7	9.6	9.7	9.8	9.7	10.3	9.9	10.0	9.7	9.5	9.7	8.7	9.1
MnO	0.1	0.1	0.2	0.1	0.2	0.2	0.2	0.2	0.2	0.2	0.2	0.2	0.1	0.2	0.2
TiO_2	3.5	3.3	3.3	3.1	2.9	2.9	3.0	3.1	3.1	3.1	3.4	2.2	3.1	1.9	1.9
total	97.6	97.9	97.9	97.6	97.5	97.6	96.8	98.3	97.2	97.1	97.2	97.0	97.3	97.0	97.2
Cl (ppm)	463	465	459	324	502	494	498	471	426	424	417	750	276	495	493
Cu (ppm)	50	60	33	37	59	50	52	37	50	56	50	11	34	4	3
H_2O (ppm)			9099	5696	9192	9807	9662	7195	8512	8125	5667	12123	6266		
S^{2-} (ppm)	815	861	738	1017	1279	1299	1133	893	953	875	569	507	970	608	602
K_2O/TiO_2	0.43	0.43	0.49	0.27	0.49	0.48	0.49	0.40	0.44	0.45	0.47	1.06	0.28	1.48	1.40
CaO/Al_2O_3	0.58	0.57	0.50	0.57	0.57	0.57	0.58	0.60	0.63	0.63	0.57	0.36	0.57	0.31	0.30
Cl/K	0.04	0.04	0.03	0.05	0.04	0.04	0.04	0.04	0.04	0.04	0.03	0.04	0.04	0.02	0.02
S^{2-}/S_{tot}	102	113	100	95	97	98	80	77	95	91	72	99	95	106	100
$\delta^{34}S$ (‰)	-1.2	-1.1	-1.0	-1.2	0.1	0.2	-1.0	-0.3	-1.2	-1.3	-1.2	0.7	-1.2	1.6	1.6
$\Delta^{33}S$ (‰)	0.017	0.017	0.027	0.030	0.020	0.028	0.025	0.021	0.028	0.012	0.031	0.007	0.028	0.027	0.026
$\Delta^{36}S$ (‰)	-0.08	-0.09	0.06	0.06	0.08	0.08	0.05	-0.01	0.13	0.08	0.06	-0.06	-0.11	0.01	0.02
$^{206}Pb/^{204}Pb$			17.747	17.926	17.742	17.742	17.749	17.791	17.816	17.809	17.770	18.1982335			
$^{207}Pb/^{204}Pb$			15.475	15.493	15.470	15.470	15.474	15.476	15.482	15.479	15.479	15.5167915			
$^{208}Pb/^{204}Pb$			38.644	38.798	38.569	38.570	38.579	38.592	38.645	38.658	38.668	38.9161373			
$^{143}Nd/^{144}Nd$			0.512537				0.512567	0.512573	0.512599	0.512583	0.512944	0.512762			
$^{87}Sr/^{86}Sr$			0.704624	0.704481	0.704483	0.704477	0.704485	0.704466	0.704482	0.704498	0.704531	0.704002			
$^{87}Sr/^{86}Sr$ [a]			0.70463	0.70447					0.70446						0.70530

a: data from bourdon et al., 2009

Table 1 – Major element, radiogenic isotopes, volatile concentration and sulfur isotope data of 15 submarine glasses from Pitcairn.

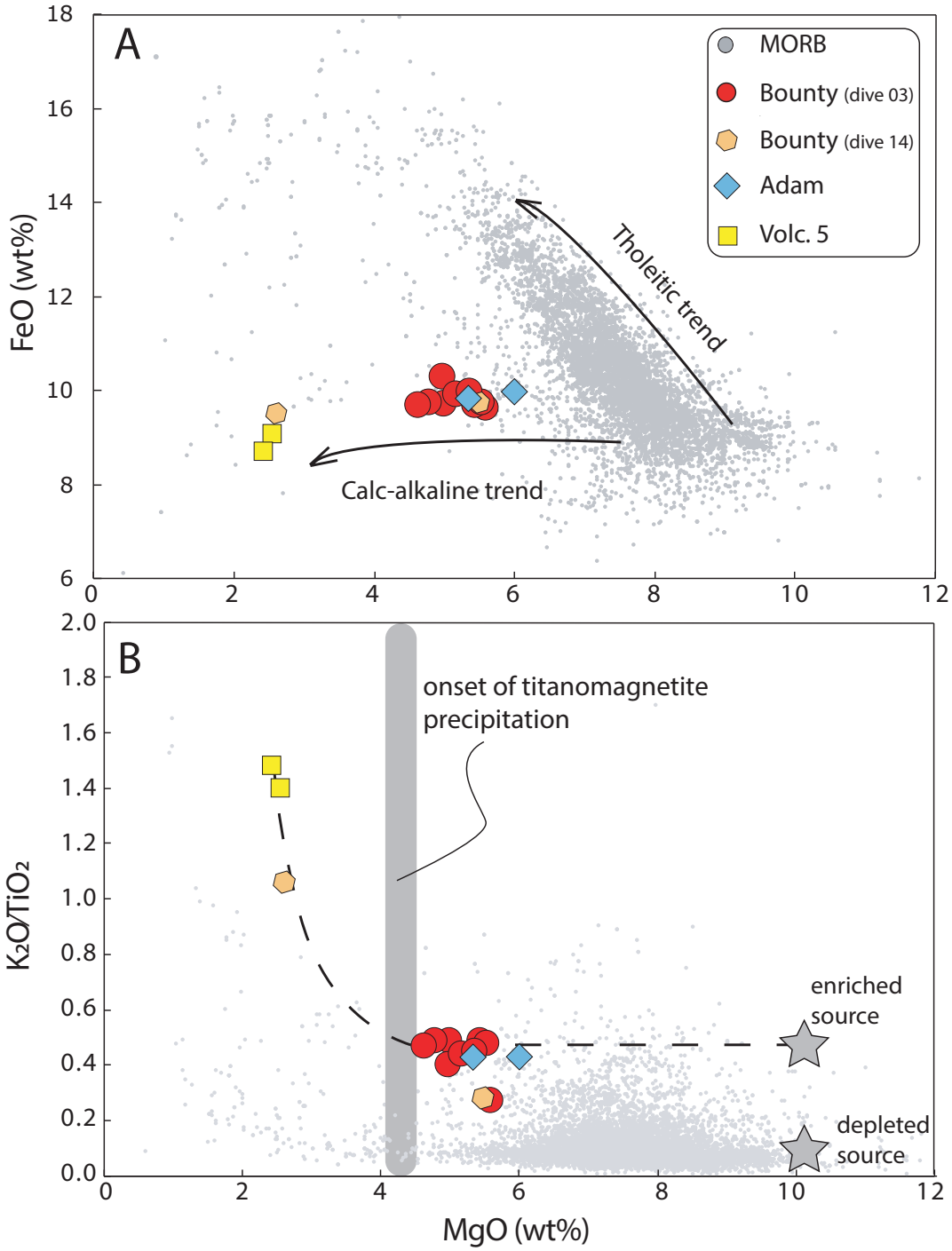

622

623 **Figure 1 –** A: iron and magnesium oxides concentrations for various basalts. B: ratio of potassium
624 to titanium oxides, shown against magnesium oxide concentrations, for various basalts. MORB data
625 are compiled using the PetDB database (www.earthchem.org/petdb, Lehnert et al., 2000). On
626 panel A, Pitcairn basalts are shown to differ from MORBs in that they undergo magmatic
627 differentiation on a calc-alkaline trend, maintaining near-constant FeO concentrations at variable
628 MgO contents. On panel B, Pitcairn basalts are shown to have rather high K_2O/TiO_2 ratios,
629 illustrating a mantle source enrichment. The onset of titanomagnetite precipitation at MgO ~4%
630 likely explains the extremely elevated K_2O/TiO_2 ratios for the most evolved basalts. A hypothetical
631 liquid line of descent is illustrated as the dashed line.

632

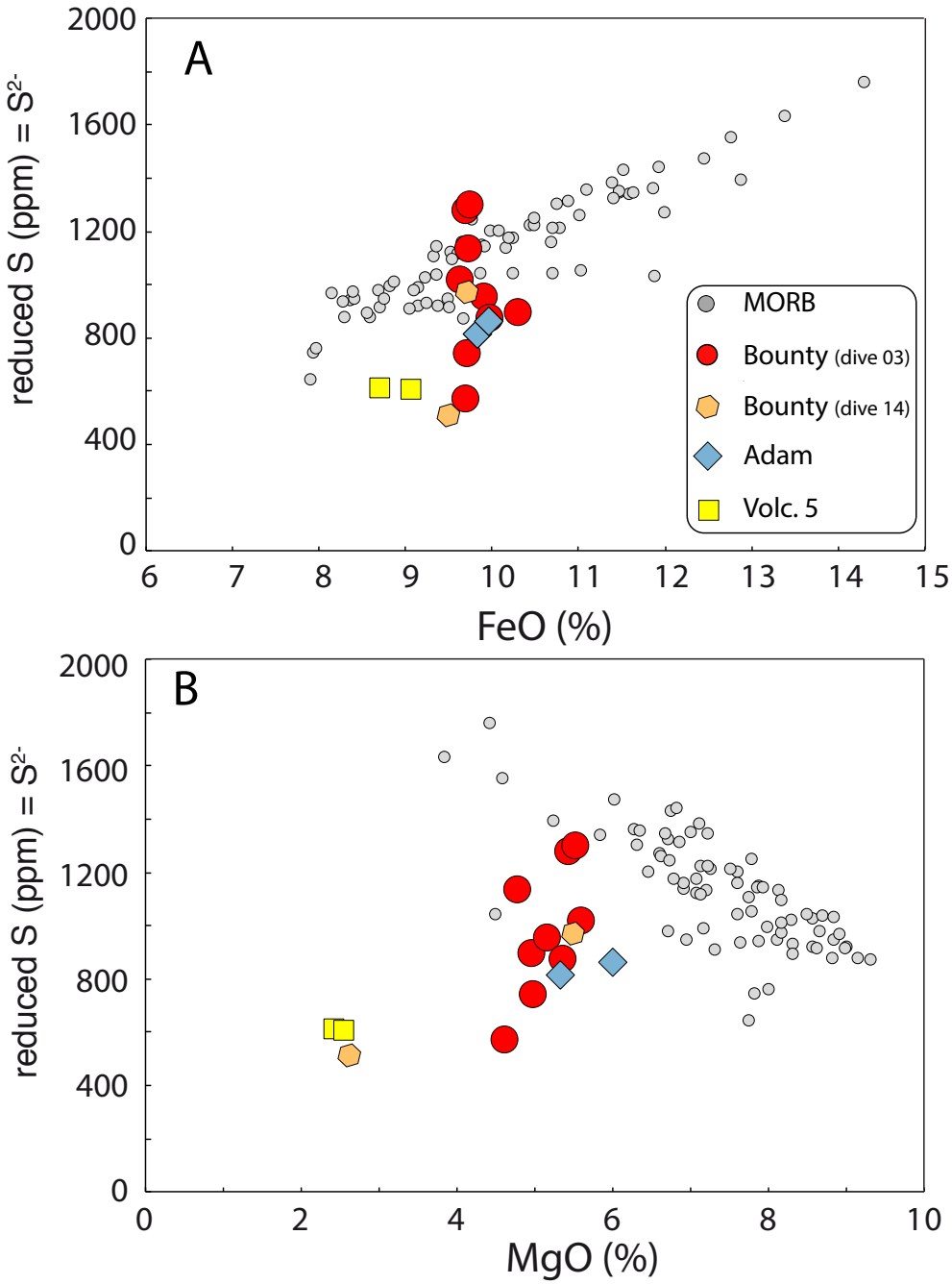

Figure 2 – reduced sulfur concentrations of MORB and Pitcairn basalts shown against A: iron and B: magnesium oxides concentrations. The error bar is MORB data acquired with the same techniques are the literature (Labidi et al., 2014, 2013). On panel A, Pitcairn basalts are shown to have a higher maximum in S solubility at a given FeO, relative to MORBs. The highest concentration of reduced sulfur observed here, at sulfide saturation, is ~1300 ± 50 ppm S at a FeO ~ 9.8 wt%. This concentration is an excess of ~ 200 ppm S relative to sulfur concentrations at sulfide saturation in tholeiitic melts (Mathez, 1976). Commonly, such high concentrations would likely be attributed to the solubility of bulk sulfur which is enhanced by sulfate occurrence (Jugo et al., 2010). Here, the high S concentration is observed in melts that appear to show limited sulfate abundances (Table 1). It is not clear whether the high S concentration illustrates the combined effects of minute sulfate abundances, magmatic temperatures and alkaline chemistry on the sulfide solubility in alkaline melts (Fortin et al., 2015). Independently of the reason for relatively high S concentrations in some of the Pitcairn melts, the near-vertical S concentrations at a given FeO (panel A) and MgO (panel B) shows sulfur loss occurred in the basalts. The sulfur loss may reflect S degassing or sulfide fractionation (see sections 5.2 and 5.3)

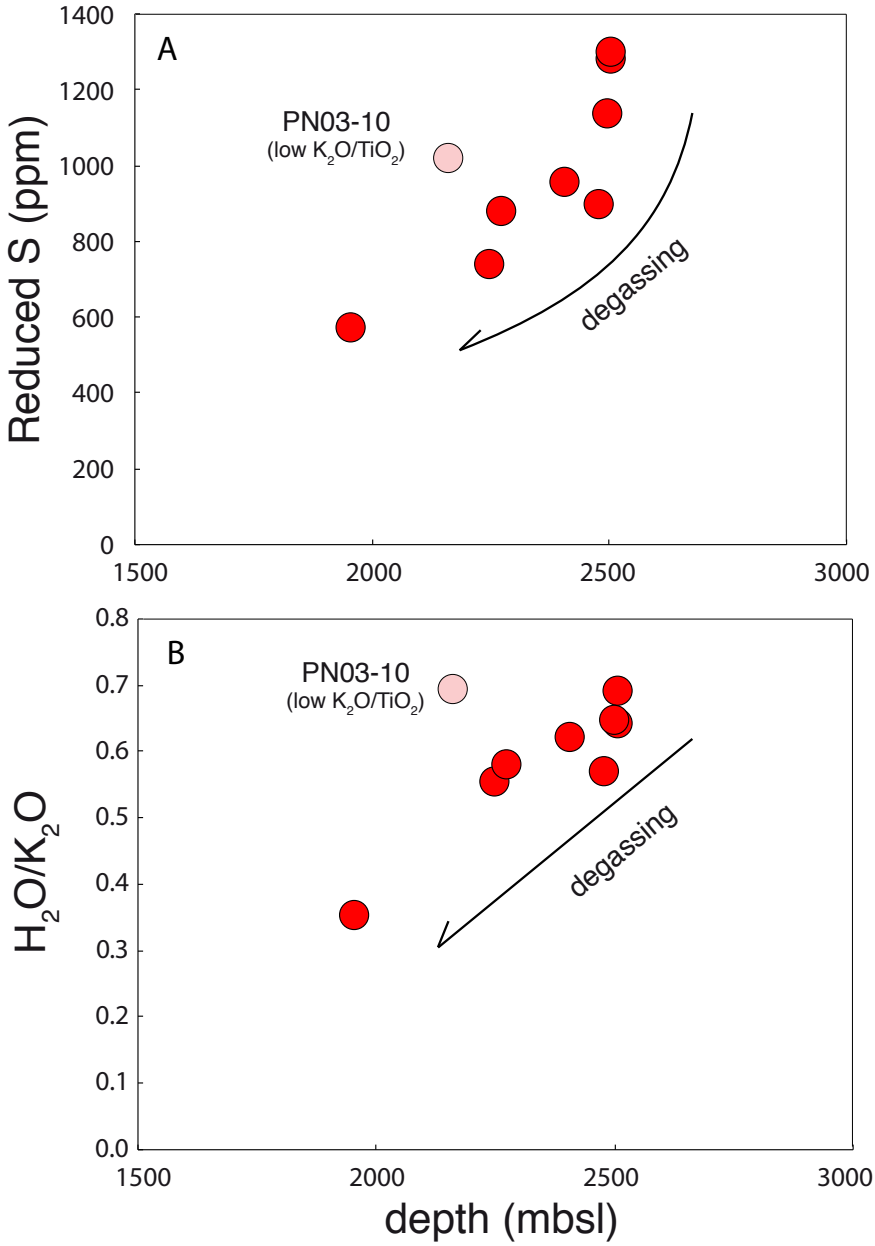

649

650 **Figure 3 –** reduced sulfur concentrations and H_2O/K_2O ratios of Pitcairn basalts from the dive 03
651 only, for which all samples have broadly homogeneous major element concentrations. For those
652 samples that were carefully picked at a given location on the flank of Bounty (Hekinian et al., 2003),
653 we assume the S concentration prior to degassing to be comparable. In contrast, we anticipate the
654 variable major element compositions of other samples from Bounty (dive 14), Adam and Volc. 5 to
655 cause variable pre-eruptive S concentration owing to the intricate link between sulfur solubility in
656 silicate melts and basalt chemistry. At a given major element concentration but variable eruption
657 depths for dive 03 basalts, the positive correlations are consistent with magmatic degassing upon
658 eruption. Only PN03-10 is an outlier. This is the only sample from this seamount with a K_2O/TiO_2
659 ratio of ~0.25, where all others have K_2O/TiO_2 ~0.45 (Fig. 1). We attribute the outlier to a distinct
660 mantle source composition in terms of volatile elements.

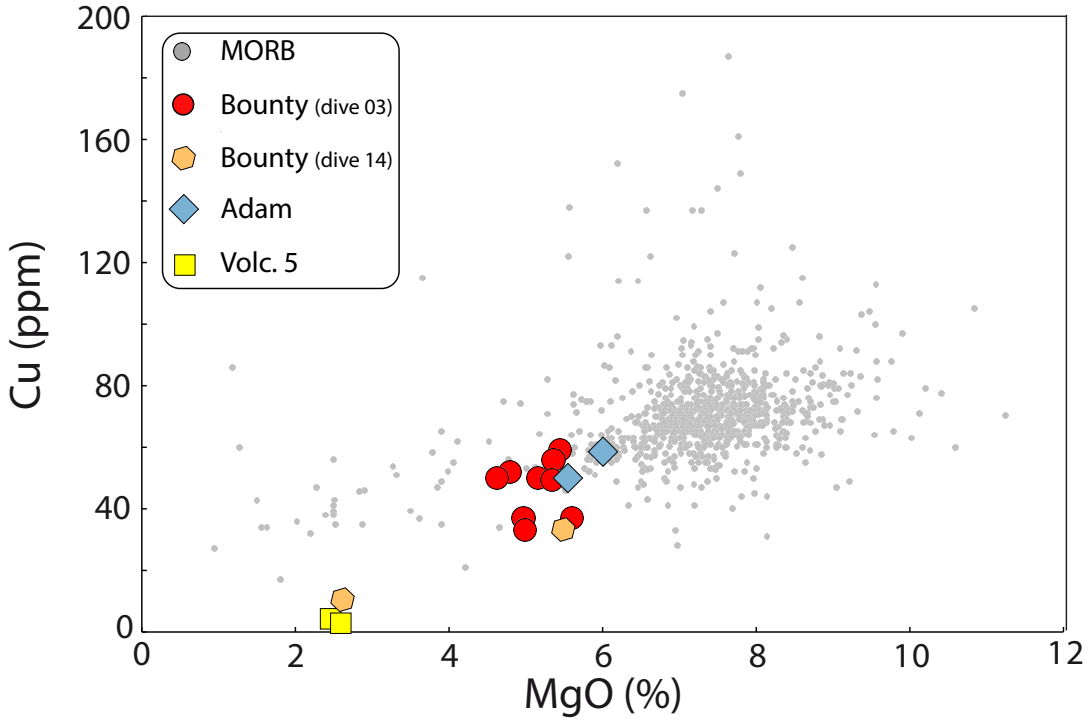

661

662 **Figure 4 –** copper concentrations of MORBs and Pitcairn basalts shown against MgO contents. The
663 Cu concentrations happen to be consistent with a MORB fractionation trend. This indicates sulfide
664 fractionation is comparable in most samples form Bounty and Adams samples.

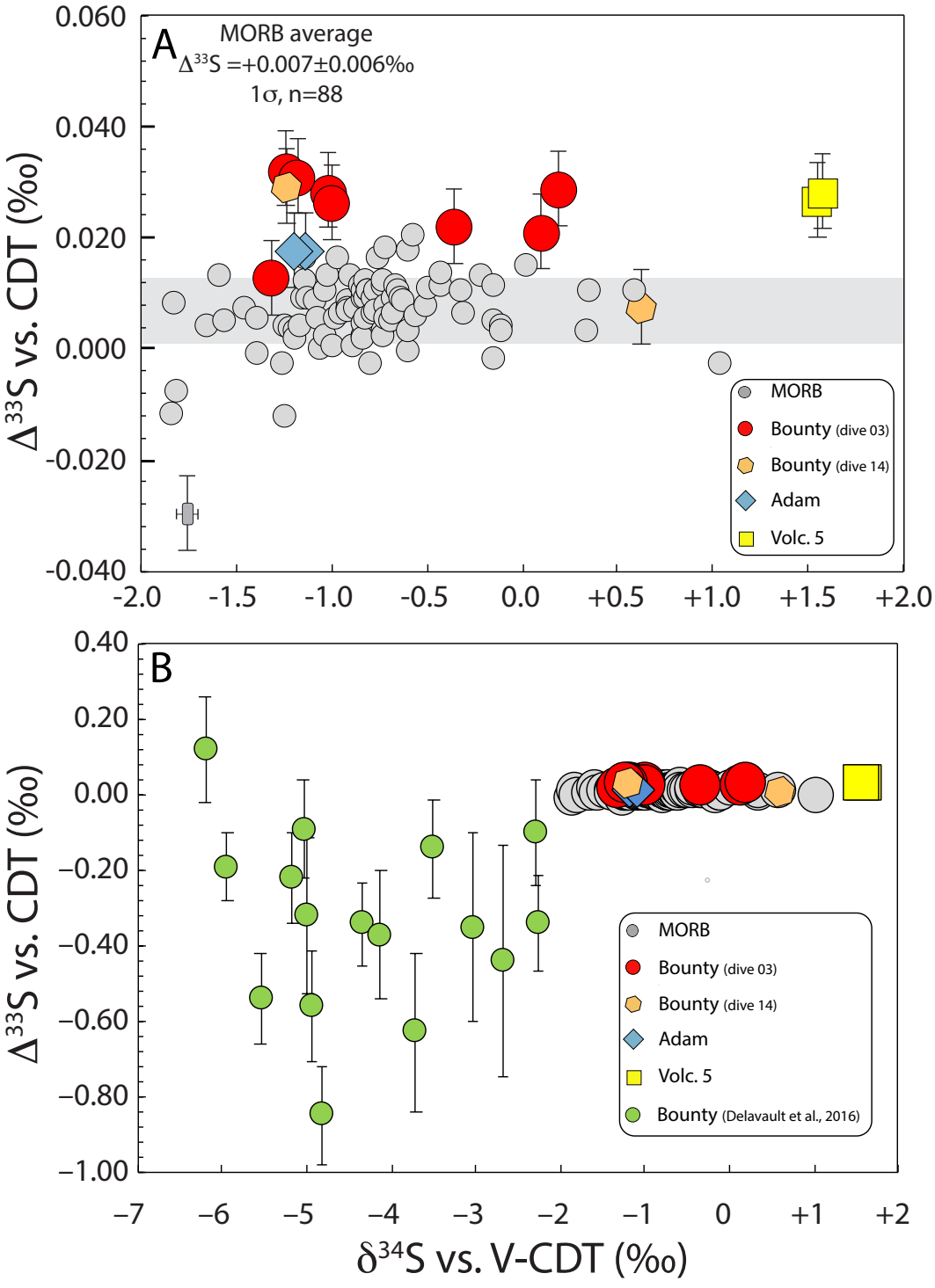

Figure 5 – $\delta^{34}S$ and $\Delta^{33}S$ of Pitcairn basalts compared to published MORB data (Labidi et al., 2014, 2013, 2012; Labidi and Cartigny, 2016). Panel A and B show the same geochemical space, but panel B incorporates the dataset from Delavault et al. (2016) obtained on individual sulfides from other basalts from the Bounty seamount. On Panel A, our data for Pitcairn basalts are shown to have an average $\Delta^{33}S$ of +0.024±0.007‰, higher than the MORB average value by ~0.02‰. the error bars of MORB measurements are shown on the bottom left. On Panel B, the data of Delavault et al., (2016) are plotted next to ours. The ion probe data from Delavault et al., (2016) show substantially negative $\Delta^{33}S$ values, down to -0.85±0.25‰, which are not duplicated by our measurements.

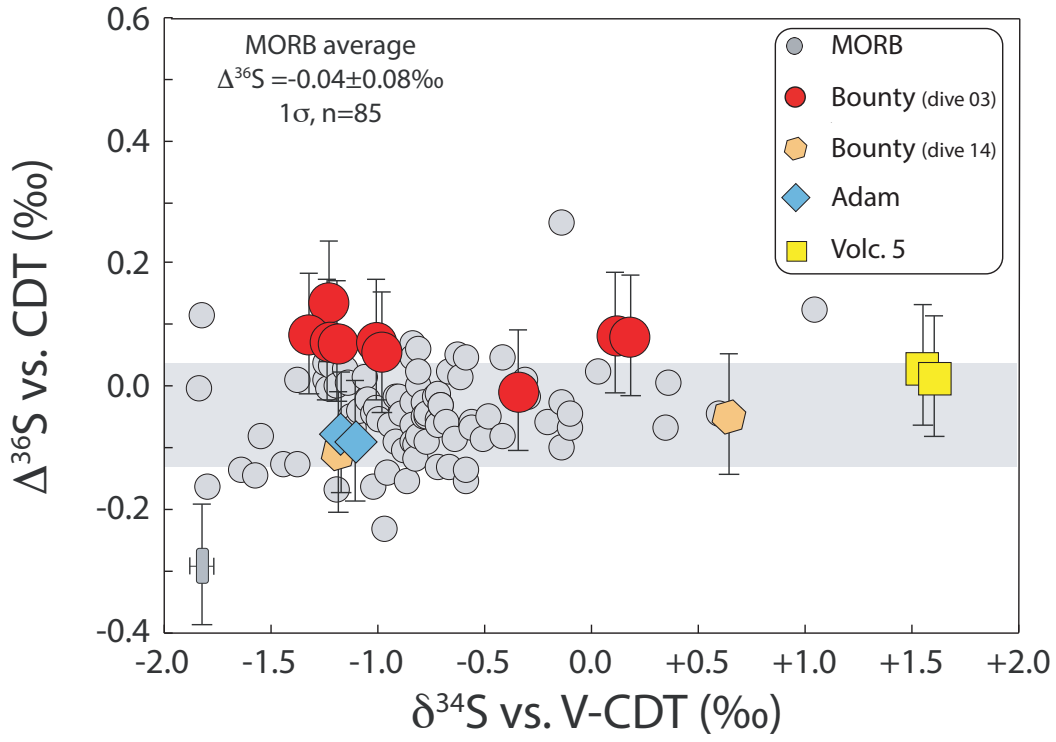

674

675 **Figure 6 –** $\delta^{34}S$ and $\Delta^{36}S$ of of Pitcairn basalts compared to published MORB data (Labidi et al.,
676 2014, 2013, 2012; Labidi and Cartigny, 2016). Pitcairn basalts show no clearly discernable ^{36}S
677 anomaly relative to MORBs.

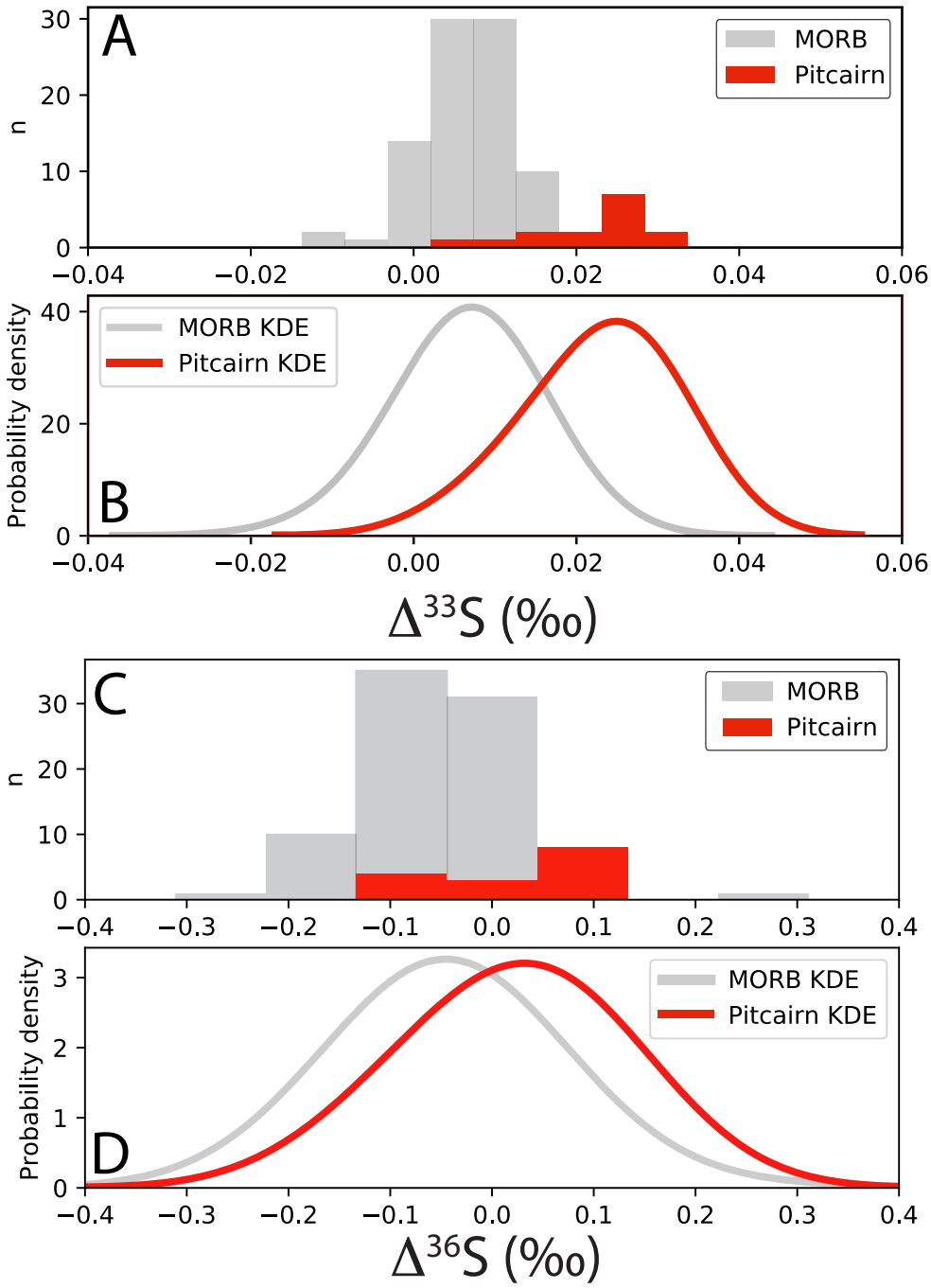

678

679 **Fig. 7 –** data distribution for ^{33}S and ^{36}S signatures of MORB and Pitcairn samples. Panels A and C
680 show data histograms and B and D show Kernel density plots (KDE), with a bandwidth equal to
681 the analytical uncertainty. Only for ^{33}S is the mean value of the Pitcairn samples statistically
682 distinct from MORB.

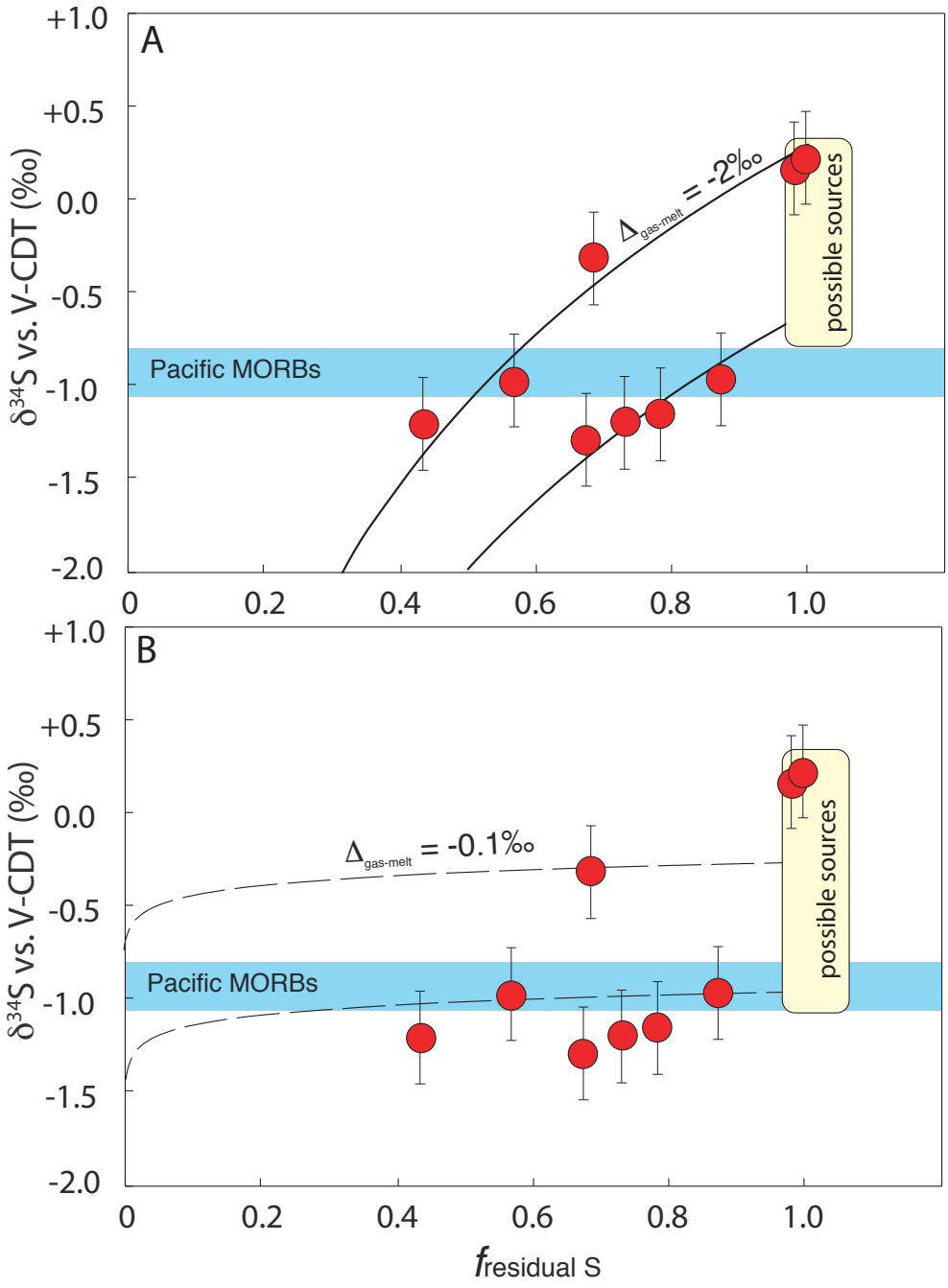

683

684 **Figure 8** – $\delta^{34}S$ values shown against the fractions of residual S^{2-} in glasses, for samples undergoing
685 varying volatile losses via degassing. Sulfur isotope ratios vary as a function of the extent of
686 degassing, recording a mass-dependent fractionation associated with volatile losses. On panel A,
687 the data are fit with a gas-melt fractionation of 2‰, consistent with S^{2-}–SO_2 equilibrium isotope
688 fractionation. Two $\delta^{34}S$ source compositions appear to be required to fit the data. They are both
689 higher than the pacific upper mantle value of -0.9±0.1‰ (Labidi et al., 2014). Alternatively, as
690 shown on panel B, the data may be fit with a gas-melt fractionation of 0.1‰, consistent with S^{2-}–
691 H_2S equilibrium isotope fractionation. In this case, three $\delta^{34}S$ source compositions would be
692 required. Most basalts would be consistent with the $\delta^{34}S$ estimate of the pacific upper mantle value.

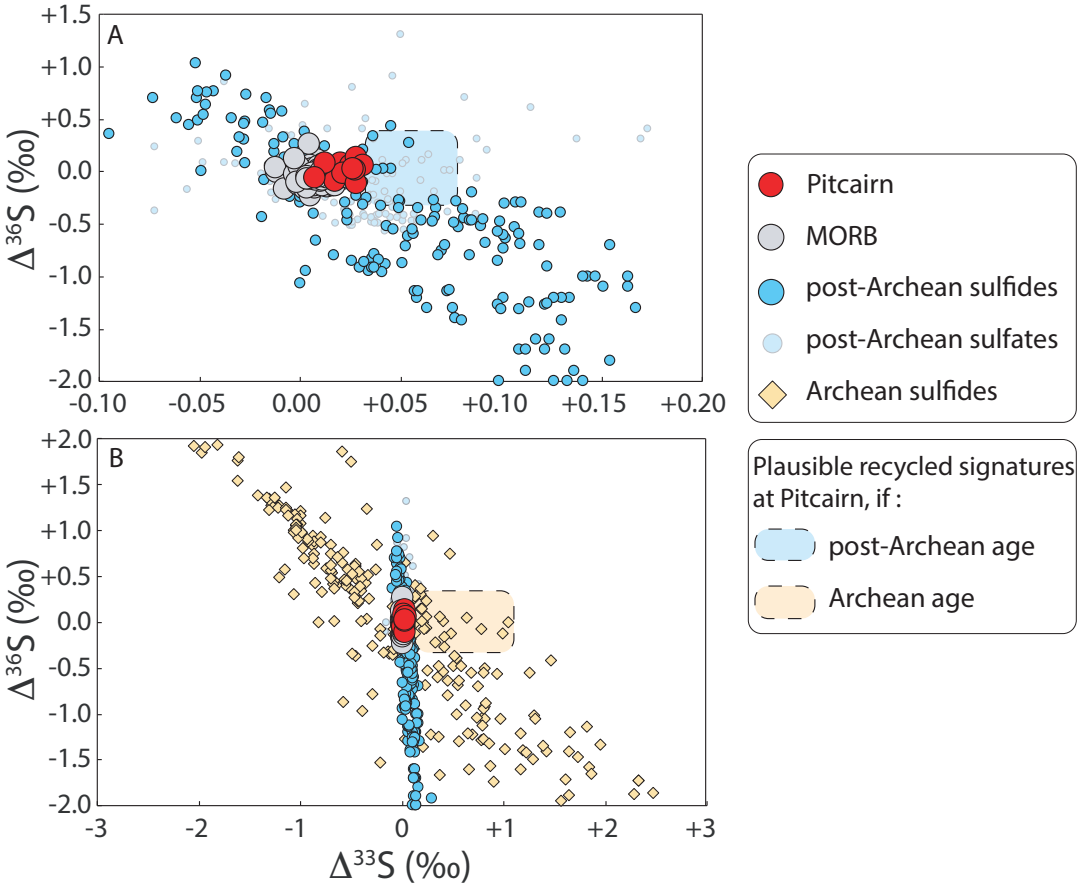

Figure 9 – Sulfur isotope ratios of Pitcairn basalts compared to MORB (data from Labidi et al., 2012, 2013, 2014, Labidi and Cartigny, 2016), Archean sediments and post-Archean sediments (data compilation from Johnston, 2011).

References

Aubaud, C., Pineau, F., Hékinian, R., Javoy, M., 2006. Carbon and hydrogen isotope constraints on degassing of CO2 and H2O in submarine lavas from the Pitcairn hotspot (South Pacific). Geophys. Res. Lett. 33.

Bourdon, B., Van Orman, J.A., 2009. Melting of enriched mantle beneath Pitcairn seamounts: Unusual U–Th–Ra systematics provide insights into melt extraction processes. Earth Planet. Sci. Lett. 277, 474–481.

Brounce, M., Stolper, E., Eiler, J., 2017. Redox variations in Mauna Kea lavas, the oxygen fugacity of the Hawaiian plume, and the role of volcanic gases in Earth's oxygenation. Proc. Natl. Acad. Sci. 114, 8997–9002.

Bucholz, C.E., Biasi, J.A., Beaudry, P., Ono, S., 2020. Sulfur isotope behavior during metamorphism and anatexis of Archean sedimentary rocks: A case study from the Ghost Lake batholith, Ontario, Canada. Earth Planet. Sci. Lett. 549, 116494.

Chauvel, C., Hofmann, A.W., Vidal, P., 1992. HIMU-EM: the French Polynesian connection. Earth Planet. Sci. Lett. 110, 99–119.

Clog, M., Aubaud, C., Cartigny, P., Dosso, L., 2013. The hydrogen isotopic composition and water content of southern Pacific MORB: A reassessment of the D/H ratio of the depleted mantle reservoir. Earth Planet. Sci. Lett. 381, 156–165. https://doi.org/http://dx.doi.org/10.1016/j.epsl.2013.08.043

715 Clog, M., Cartigny, P., Aubaud, C., 2012. Experimental evidence for interaction of water vapor and platinum
716 crucibles at high temperatures: Implications for volatiles from igneous rocks and minerals. Geochim.
717 Cosmochim. Acta 83, 125–137.

718 Danyushevsky, L. V, 2001. The effect of small amounts of H2O on crystallisation of mid-ocean ridge and
719 backarc basin magmas. J. Volcanol. Geotherm. Res. 110, 265–280.

720 Delavault, H., Chauvel, C., Thomassot, E., Devey, C.W., Dazas, B., 2016. Sulfur and lead isotopic evidence of
721 relic Archean sediments in the Pitcairn mantle plume. Proc. Natl. Acad. Sci. 113, 12952–12956.

722 Dixon, J.E., Clague, D.A., Stolper, E.M., 1991. Degassing history of water, sulfur, and carbon in submarine
723 lavas from Kilauea Volcano, Hawaii. J. Geol. 99, 371–394.

724 Dixon, J.E., Leist, L., Langmuir, C., Schilling, J.-G., 2002. Recycled dehydrated lithosphere observed in plume-
725 influenced mid-ocean-ridge basalt. Nature 420, 385–389.

726 Dottin III, J., Labidi, J., Jackson, M.G., Woodhead, J., Farquhar, J., 2020a. Isotopic Evidence for Multiple
727 Recycled Sulfur Reservoirs in the Mangaia Mantle Plume. Geochemistry, Geophys. Geosystems 21.
728 https://doi.org/10.1029/2020GC009081

729 Dottin III, J., Labidi, J., Lekic, V., Jackson, M.G., Farquhar, J., 2020b. Sulfur isotope characterization of
730 primordial and recycled sources feeding the Samoan mantle plume. Earth Planet. Sci. Lett. 534,
731 116073.

732 Eisele, J., Sharma, M., Galer, S.J.G., Blichert-Toft, J., Devey, C.W., Hofmann, A.W., 2002. The role of sediment
733 recycling in EM-1 inferred from Os, Pb, Hf, Nd, Sr isotope and trace element systematics of the Pitcairn
734 hotspot. Earth Planet. Sci. Lett. 196, 197–212.

735 Farquhar, J., Peters, M., Johnston, D.T., Strauss, H., Masterson, A., Wiechert, U., Kaufman, A.J., 2007. Isotopic
736 evidence for Mesoarchaean anoxia and changing atmospheric sulphur chemistry. Nature 449, 706–
737 709.

738 Fortin, M.-A., Riddle, J., Desjardins-Langlais, Y., Baker, D.R., 2015. The effect of water on the sulfur
739 concentration at sulfide saturation (SCSS) in natural melts. Geochim. Cosmochim. Acta 160, 100–116.
740 https://doi.org/http://dx.doi.org/10.1016/j.gca.2015.03.022

741 Gibson, S.A., Thompson, R.N., Day, J.A., Humphris, S.E., Dickin, A.P., 2005. Melt-generation processes
742 associated with the Tristan mantle plume: Constraints on the origin of EM-1. Earth Planet. Sci. Lett.
743 237, 744–767.

744 Hart, S.R., Gerlach, D.C., White, W.M., 1986. A possible new Sr-Nd-Pb mantle array and consequences for
745 mantle mixing. Geochim. Cosmochim. Acta 50, 1551–1557.

746 Hekinian, R., Cheminée, J.L., Dubois, J., Stoffers, P., Scott, S., Guivel, C., Garbe-Schönberg, D., Devey, C.,
747 Bourdon, B., Lackschewitz, K., 2003. The Pitcairn hotspot in the South Pacific: distribution and
748 composition of submarine volcanic sequences. J. Volcanol. Geotherm. Res. 121, 219–245.

749 Hoernle, K., Hauff, F., Werner, R., van den Bogaard, P., Gibbons, A.D., Conrad, S., Müller, R.D., 2011. Origin of
750 Indian Ocean Seamount Province by shallow recycling of continental lithosphere. Nat. Geosci. 4, 883–
751 887.

752 Hofmann, A.W., White, W.M., 1982. Mantle plumes from ancient oceanic crust. Earth Planet. Sci. Lett. 57,
753 421–436.

754 Honda, M., Woodhead, J.D., 2005. A primordial solar-neon enriched component in the source of EM-I-type
755 ocean island basalts from the Pitcairn Seamounts, Polynesia. Earth Planet. Sci. Lett. 236, 597–612.

756 Jackson, M.G., Dasgupta, R., 2008. Compositions of HIMU, EM1, and EM2 from global trends between
757 radiogenic isotopes and major elements in ocean island basalts. Earth Planet. Sci. Lett. 276, 175–186.

758 Jenner, F.E., O'Neill, H.S.T.C., Arculus, R.J., Mavrogenes, J.A., 2010. The magnetite crisis in the evolution of arc-
759 related magmas and the initial concentration of Au, Ag and Cu. J. Petrol. 51, 2445–2464.

760 Johnston, D.T., 2011. Multiple sulfur isotopes and the evolution of Earth's surface sulfur cycle. Earth-Science
761 Rev. 106, 161–183.

762 Jugo, P.J., Wilke, M., Botcharnikov, R.E., 2010. Sulfur K-edge XANES analysis of natural and synthetic basaltic

763 glasses: Implications for S speciation and S content as function of oxygen fugacity. Geochim.
764 Cosmochim. Acta 74, 5926–5938.

765 Labidi, J., Cartigny, P., 2016. Negligible sulfur isotope fractionation during partial melting: Evidence from
766 Garrett transform fault basalts, implications for the late-veneer and the hadean matte. Earth Planet.
767 Sci. Lett. 451. https://doi.org/10.1016/j.epsl.2016.07.012

768 Labidi, J., Cartigny, P., Birck, J.L., Assayag, N., Bourrand, J.J., 2012. Determination of multiple sulfur isotopes
769 in glasses: A reappraisal of the MORB $\delta^{34}S$. Chem. Geol. 334.
770 https://doi.org/10.1016/j.chemgeo.2012.10.028

771 Labidi, J., Cartigny, P., Hamelin, C., Moreira, M., Dosso, L., 2014. Sulfur isotope budget (^{32}S, ^{33}S, ^{34}S and ^{36}S)
772 in Pacific-Antarctic ridge basalts: A record of mantle source heterogeneity and hydrothermal sulfide
773 assimilation. Geochim. Cosmochim. Acta 133. https://doi.org/10.1016/j.gca.2014.02.023

774 Labidi, J., Cartigny, P., Moreira, M., 2013. Non-chondritic sulphur isotope composition of the terrestrial
775 mantle. Nature 501. https://doi.org/10.1038/nature12490

776 Lee, C.-T.A., Luffi, P., Chin, E.J., Bouchet, R., Dasgupta, R., Morton, D.M., Le Roux, V., Yin, Q., Jin, D., 2012.
777 Copper systematics in arc magmas and implications for crust-mantle differentiation. Science (80-.).
778 336, 64–68.

779 Lehnert, K., Su, Y., Langmuir, C.H., Sarbas, B., Nohl, U., 2000. A global geochemical database structure for
780 rocks. Geochemistry, Geophys. Geosystems 1.

781 Lorand, J.-P., Luguet, A., 2016. Chalcophile and siderophile elements in mantle rocks: Trace elements
782 controlled by trace minerals. Rev. Mineral. Geochemistry 81, 441–488.

783 Mathez, E.A., 1976. Sulfur solubility and magmatic sulfides in submarine basalt glass. J. Geophys. Res. 81,
784 4269–4276.

785 McKenzie, D., O'nions, R.K., 1983. Mantle reservoirs and ocean island basalts. Nature 301, 229–231.

786 McKenzie, D.A.N., O'Nions, R.K., 1995. The source regions of ocean island basalts. J. Petrol. 36, 133–159.

787 Michael, P., 1995. Regionally distinctive sources of depleted MORB: Evidence from trace elements and H2O.
788 Earth Planet. Sci. Lett. 131, 301–320.

789 Michael, P.J., Cornell, W.C., 1998. Influence of spreading rate and magma supply on crystallization and
790 assimilation beneath mid-ocean ridges: Evidence from chlorine and major element chemistry of mid-
791 ocean ridge basalts. J. Geophys. Res. Solid Earth 103, 18325–18356.

792 Michael, P.J., Schilling, J.-G., 1989. Chlorine in mid-ocean ridge magmas: evidence for assimilation of
793 seawater-influenced components. Geochim. Cosmochim. Acta 53, 3131–3143.

794 Mougel, B., Agranier, A., Hemond, C., Gente, P., 2014. A highly unradiogenic lead isotopic signature revealed
795 by volcanic rocks from the East Pacific Rise. Nat. Commun. 5, 1–7.

796 Mukhopadhyay, S., 2012. Early differentiation and volatile accretion recorded in deep-mantle neon and
797 xenon. Nature 486, 101–104. https://doi.org/10.1038/nature11141

798 Mukhopadhyay, S., Parai, R., 2019. Noble gases: a record of Earth's evolution and mantle dynamics. Annu.
799 Rev. Earth Planet. Sci. 47, 389–419.

800 Nielsen, S.G., Shimizu, N., Lee, C.A., Behn, M.D., 2014. Chalcophile behavior of thallium during MORB melting
801 and implications for the sulfur content of the mantle. Geochemistry, Geophys. Geosystems 15, 4905–
802 4919.

803 Parai, R., Mukhopadhyay, S., Tucker, J.M., Pető, M.K., 2019. The emerging portrait of an ancient,
804 heterogeneous and continuously evolving mantle plume source. Lithos 346, 105153.

805 Plank, T., Langmuir, C.H., 1998. The chemical composition of subducting sediment and its consequences for
806 the crust and mantle. Chem. Geol. 145, 325–394.

807 Poulton, S.W., Fralick, P.W., Canfield, D.E., 2004. The transition to a sulphidic ocean~ 1.84 billion years ago.
808 Nature 431, 173–177.

809 Reinhard, C.T., Planavsky, N.J., Lyons, T.W., 2013. Long-term sedimentary recycling of rare sulphur isotope
810 anomalies. Nature 497, 100–103.

811 Rudnick, R.L., Gao, S., Holland, H.D., Turekian, K.K., 2003. Composition of the continental crust. The crust 3,
812 1–64.

813 Sobolev, A. V, Chaussidon, M., 1996. H2O concentrations in primary melts from supra-subduction zones and
814 mid-ocean ridges: implications for H2O storage and recycling in the mantle. Earth Planet. Sci. Lett.
815 137, 45–55.

816 Turner, S.J., Langmuir, C.H., Dungan, M.A., Escrig, S., 2017. The importance of mantle wedge heterogeneity to
817 subduction zone magmatism and the origin of EM1. Earth Planet. Sci. Lett. 472, 216–228.

818 Wedepohl, K.H., 1995. The composition of the continental crust. Geochim. Cosmochim. Acta 59, 1217–1232.

819 Weis, D., Garcia, M.O., Rhodes, J.M., Jellinek, M., Scoates, J.S., 2011. Role of the deep mantle in generating the
820 compositional asymmetry of the Hawaiian mantle plume. Nat. Geosci. 4, 831–838.

821 Willbold, M., Stracke, A., 2006. Trace element composition of mantle end-members: Implications for
822 recycling of oceanic and upper and lower continental crust. Geochemistry, Geophys. Geosystems 7.

823 Woodhead, J.D., Devey, C.W., 1993. Geochemistry of the Pitcairn seamounts, I: source character and
824 temporal trends. Earth Planet. Sci. Lett. 116, 81–99.

825 Woodhead, J.D., Greenwood, P., Harmon, R.S., Stoffers, P., 1993. Oxygen isotope evidence for recycled crust
826 in the source of EM-type ocean island basalts. Nature 362, 809–813.

827 Workman, R.K., Hauri, E., Hart, S.R., Wang, J., Blusztajn, J., 2006. Volatile and trace elements in basaltic
828 glasses from Samoa: Implications for water distribution in the mantle. Earth Planet. Sci. Lett. 241,
829 932–951.

830 Yierpan, A., König, S., Labidi, J., Schoenberg, R., 2019. Selenium isotope and S-Se-Te elemental systematics
831 along the Pacific-Antarctic ridge: Role of mantle processes. Geochim. Cosmochim. Acta 249.
832 https://doi.org/10.1016/j.gca.2019.01.028

833 Zimmer, M.M., Plank, T., Hauri, E.H., Yogodzinski, G.M., Stelling, P., Larsen, J., Singer, B., Jicha, B., Mandeville,
834 C., Nye, C.J., 2010. The role of water in generating the calc-alkaline trend: new volatile data for
835 Aleutian magmas and a new tholeiitic index. J. Petrol. 51, 2411–2444.

836 Zindler, A., Hart, S., 1986. Chemical geodynamics. Annu. Rev. Earth Planet. Sci. 14, 493–571.

837

838

839